

## A Study on CO<sub>2</sub> Sorption Coefficient and Compatibility of Blend Mixed Matrix Membrane

Suhan Selvarajoo,<sup>1</sup> Zeinab Abbas Jawad,<sup>2\*</sup> Swee Pin Yeap,<sup>3</sup> Ahmed M. Elkhatat,<sup>2</sup>  
Anas Khalid Abdelsalam Abdelgadir<sup>2</sup> and Vahid Khosravi<sup>3</sup>

<sup>1</sup>Department of Chemical and Energy Engineering, Faculty of Engineering and Science,  
Curtin University Malaysia, 250CDT, 98009 Miri, Sarawak, Malaysia

<sup>2</sup>Department of Chemical Engineering, College of Engineering, Qatar University,  
P.O Box 2713, Doha, Qatar

<sup>3</sup>Department of Chemical and Petroleum Engineering, UCSI University, Cheras,  
56000 Kuala Lumpur, Malaysia

\*Corresponding author: zjawad@qu.edu.qa

Published online: 21 April 2025

To cite this article: Selvarajoo, S. et al. (2025). A study on CO<sub>2</sub> sorption coefficient and compatibility of blend mixed matrix membrane. *J. Phys. Sci.*, 36(1), 55–70. <https://doi.org/10.21315/jps2025.36.1.5>

To link to this article: <https://doi.org/10.21315/jps2025.36.1.5>

**ABSTRACT:** *Presently, the power generation industry has grown in response to the rising demand for electricity, resulting in higher reliance on the combustion of fossil fuels and coals. As a consequence, this has greatly impacted global warming causing an increase in the emission of carbon dioxide (CO<sub>2</sub>), which in turn has affected the sustainable development goals globally. There are several carbon capture methods used in the industries with the aim of reducing the emission of CO<sub>2</sub>. One of the most popular membrane technology methods is Mixed Matrix Membranes (MMMs). In this research, the blend MMMs were synthesised by embedding the functionalised multi-walled carbon nanotubes (MWCNTs-F) using Chen's Soft-Cutting method along with  $\beta$ -cyclodextrin ( $\beta$ -CD) into the blend cellulose acetate butyrate (CAB) polymer, which had different molecular weights of 12,000, 16,000 and 70,000, mixed in a ratio of 1:2:2. To date, the Hansen solubility parameters together with the CO<sub>2</sub> solubility and diffusivity coefficients have not been explored for this combination of MMMs. However, this work demonstrated the CO<sub>2</sub> solubility coefficient directly correlate to the CO<sub>2</sub> permeance of MMM. Additionally, the CO<sub>2</sub> coefficient was influenced by chain spacing and the amorphous fraction, which in turn affected the CO<sub>2</sub> affinity of the membrane.*

**Keywords:** CO<sub>2</sub> solubility coefficient, Hansen solubility parameter, blend cellulose acetate butyrate, functionalised MWCNTs, CO<sub>2</sub> permeance

## 1. INTRODUCTION

Membrane technology is an efficient and state-of-the-art technology for separation processes because it offers several advantages compared to other technologies.<sup>1-3</sup> Numerous studies have shown that membrane technology is reliable based on the performance of the results.<sup>4-7</sup> The Cellulose Acetate Butyrate (CAB) polymer has some key characteristics such as highly available, biodegradable, resistance towards acid, alkali and organic solvents as well as extremely stable and durable as a polymer.<sup>8-10</sup> Most importantly, CAB demonstrates high carbon dioxide (CO<sub>2</sub>) gas permeability attributed to the presence of the butyryl and acetyl groups.<sup>11-13</sup> Therefore, CAB is regarded as a superior cellulose material when compared to CA, mainly due to these acetyl and butyrate groups. On the other hand, when multi-walled carbon nanotubes (MWCNTs) are integrated as inorganic fillers, mixed matrix membranes (MMMs) are synthesised with CAB, resulting in CO<sub>2</sub> separation from flue gas due to the non-covalent functionalisation of MWCNTs.<sup>11</sup> The MWCNTs have the tendency to increase the permeance of CO<sub>2</sub> molecules owing to their remarkable durability and capacity for absorption.<sup>14</sup> Moreover, CO<sub>2</sub> has a higher solubility tendency in a CAB polymer membrane compared to other gases.<sup>15,16</sup>

However, the properties of the MMM polymer can be influenced when using different molecular weights. To fabricate a blend CAB/MWCNTs membrane with high efficiency, three different molecular weights (Mn) of 12,000, 16,000 and 70,000—were proposed for the CAB and in accordance to Manimaran et al.<sup>17</sup> They found that blending these three polymers together influenced the rheology, thereby driving a notable improvement in the performance of the CAB blend membrane. Moreover, the carbonyl (C=O) and hydroxyl (O-H) groups raised the hydrophilicity of the blend polymers, which enhanced its affinity towards non-polar CO<sub>2</sub>. This interaction promoted the CO<sub>2</sub> permeance through the membrane.<sup>18</sup> The addition of inorganic fillers like the MWCNTs significantly influence the properties and morphology of MMMs.<sup>19</sup> The MWCNTs possess a unique hollow structure and smooth inner walls, which act as “nanochannels” when integrated into the polymer matrix. These channels provide a pathway for gas molecules to permeate through the membrane, enhancing gas separation efficiency. However, the incorporation of MWCNTs also alter the polymer chain conformation and packing near the membrane surface, thereby affecting the overall membrane morphology.<sup>20</sup> Excessive loading alters the membrane’s performance by disrupting the polymer matrix and potentially leading to defects, while insufficient loading may limit the enhancement of gas separation properties.<sup>21</sup> Therefore, loading of the MWCNT is essential to maximise the benefits of fillers in MMMs for gas separation applications.

Recently, the Hansen solubility parameter (HSP) has been used to ascertain the nature of the interactive forces and assess the compatibility of materials. The HSP is based on the cohesive energy of the material and is categorised into three parts, namely atomic dispersion ( $\delta_d$ ), molecular dipolar interaction ( $\delta_p$ ) and hydrogen-bonding interaction ( $\delta_h$ ). This approach is essential for studying and exploring the solubility theory of solvents, polymers and inorganic fillers. In a HSP plot, when the distance between components decreases, it leads to a notable increase in solubility, resulting in an improved CO<sub>2</sub> permeance.<sup>22, 23</sup>

Based on the above, significant research has been conducted on the blending of CAB polymer and MWCNTs. However, to date, no work has been conducted to study the synergistic effects of the compatibility using HSP and sorption study including CO<sub>2</sub> solubility and diffusivity coefficient of MMM (CAB/MWCNTs), for gas separation. Thus, the aim of this research is to explore the blending of CAB synthesised with molecular weights of 12,000, 16,000 and 70,000 in a ratio of 1:2:2, respectively with varying loadings of MWCNTs-F.

## **2. MATERIALS AND EXPERIMENTAL METHODOLOGY**

### **2.1 Materials**

The CAB polymer with Mn of 12,000, 16,000 and 70,000 and acetyl content of 12 wt.% to 15 wt.% were procured from Sigma Aldrich (Malaysia). The chloroform solvent (97%) was purchased from Merck (Malaysia) while isopropyl alcohol (99.6%) and hexane (99.8%) were obtained from Merck (Malaysia) for membrane drying purposes. The purified CO<sub>2</sub> was supplied by Linde EOX Sdn. Bhd. (Malaysia). The beta-cyclodextrin ( $\beta$ -CD) was also purchased from Merck (Malaysia). The MWCNTs (95%) were sourced from Shenzhen Nanotech China Port Co. with an average outer diameter of 26.62 nm and an inner diameter of 8.85 nm. Additionally, the ethanol (99.5%) was obtained from Merck (Malaysia) for the purpose of functionalisation of MWCNTs.

### **2.2 Functionalisation of MWCNTs-F**

The functionalisation of MWCNTs commenced with conditions of drying to eradicate moisture at a temperature of 120°C for approximately 12 h. To minimise structural damage and preserve the desired properties of the MWCNTs, Chen's Soft-Cutting Method was used to functionalise the dried MWCNTs.<sup>24,25</sup> The pristine-MWCNTs(MWCNTs-P) were pounded with a pestle and mortar under conditions where the concentration ratio was at 1:30 wt.% of  $\beta$ -CD. The use of  $\beta$ -CD is essential to keep the CNTs evenly spread within the polymer matrix of

the MMM.<sup>26</sup> During the first 10 min of the process, 185.2 mL of ethanol was added gradually to form a sticky lightgrey mixture. The grinding process resumed for another 2.5 h until the result turned into a fine powder, which was then heated at 80°C in the oven for one day.<sup>11</sup>

### 2.3 Fabrication of MMM

The MMM was fabricated using the wet-phase inversion method.<sup>27</sup> A process that transforms a homogeneous polymer solution from a liquid to a solid state. This transformation occurs through precipitation, driven by solvent-nonsolvent exchange during immersion in a coagulation bath.<sup>28</sup> Solid base MWCNTs-F were added to the chloroform and sonicated for approximately 20 min. Subsequently, a magnetic stirrer was used to stir the mixture for 4 h to ensure that the distribution of particles was well dispersed. Next, the CAB polymer together with the chloroform was added to the MWCNTs-F. This mixture was stirred for a full day until the CAB polymer was evenly distributed in the mixture.<sup>11</sup> Further, the thickness of the casting knife was aligned at 250  $\mu\text{m}$  for all the membranes. Next, the membrane was cast onto a glass plate using an automatic film machine (PLC Solution, Malaysia) and left for 5 min–10 min to allow the solvent to evaporate. It was then immersed in distilled water at room temperature (23°C–25°C) for 24 h.<sup>11</sup> The solvent-exchange drying method was then performed to eradicate any trace of water present in the membrane's structure by submerging the membrane in isopropyl for 30 min. Subsequently, the fabricated membrane was immersed into n-hexane for another 30 min. After immersing the membrane in isopropyl followed by n-hexane, it was dried by fitting it between two glass plates with filter papers for 24 h at room temperature to remove any remaining volatile liquid.<sup>11</sup> Table 1 summarises the composition for each membrane.

Table 1: The composition of membrane fabricated at different loadings of MWCNTs-F.

| CAB<br>wt. % | Chloroform<br>wt. % | Total fillers<br>wt. % | MWCNTs<br>wt. % | $\beta$ -CD<br>wt. % | Casting<br>thickness, $\mu\text{m}$ | Sample<br>name |
|--------------|---------------------|------------------------|-----------------|----------------------|-------------------------------------|----------------|
| 4            | 95.87               | 0.1                    | 0.0041          | 0.124                | 250                                 | M-0.1          |
| 4            | 95.74               | 0.2                    | 0.0085          | 0.256                | 250                                 | M-0.2          |
| 4            | 95.59               | 0.3                    | 0.0133          | 0.398                | 250                                 | M-0.3          |
| 4            | 95.43               | 0.4                    | 0.0182          | 0.548                | 250                                 | M-0.4          |
| 4            | 95.26               | 0.5                    | 0.0237          | 0.710                | 250                                 | M-0.5          |

## 2.4 Hansen Solubility Parameters

The positions of solvents, polymers and inorganic fillers are observed by plotting a ternary diagram. This diagram utilises the normalised values of HSP to convert the dispersion ( $\delta_d$ ), polar ( $\delta_p$ ) and hydrogen components ( $\delta_h$ ) into a simplified two-dimensional graph. In this ternary diagram, the left axis represents dispersion (D), the lower axis represents polarity (P) and the right axis represents hydrogen bonding (H).<sup>22</sup>

The values that are available in the HSP database online are the absolute HSP values. However, the ternary graph uses normalised HSP values. Equation (1) to Equation (3) convert the absolute HSP values into the normalised HSP values.<sup>23</sup>

$$\%d \text{ Norm} = \frac{\delta d}{\delta d + \delta p + \delta h} \times 100\% \quad (1)$$

$$\%p \text{ Norm} = \frac{\delta p}{\delta d + \delta p + \delta h} \times 100\% \quad (2)$$

$$\%h \text{ Norm} = \frac{\delta h}{\delta d + \delta p + \delta h} \times 100\% \quad (3)$$

In the ternary diagram, the primary study of HSP is the distances between materials, known as relative affinity, which ascertains the compatibility of materials. Equation (4) to Equation (5) are used to calculate the relative affinity in two and three components.<sup>29</sup>

Two components (A and B)

$$\text{Relative affinity of } AB = \sqrt{(\delta_{dA} - \delta_{dB})^2 + (\delta_{hA} - \delta_{hB})^2 + (\delta_{pA} - \delta_{pB})^2} \quad (4)$$

Three components (A, B and C)

$$\begin{aligned} \text{Relative affinity of } AC - BC = \\ \frac{(\sqrt{(\delta_{dA} - \delta_{dC})^2 + (\delta_{hA} - \delta_{hC})^2 + (\delta_{pA} - \delta_{pC})^2})}{(\sqrt{(\delta_{dB} - \delta_{dC})^2 + (\delta_{hB} - \delta_{hC})^2 + (\delta_{pB} - \delta_{pC})^2})} \end{aligned} \quad (5)$$

## 2.5 Membrane Permeation Test

The performance of the membrane was evaluated using the volume displacement method.<sup>17</sup>

## 2.6 Gas Separation Performance

The following equations and formulas were used to determine the gas permeation and separation performance as well as the flux of the gas sample,  $N_i$ .<sup>30</sup>

$$N_i = \frac{\text{mol of components gas } A \text{ permeating through membrane}}{t_{AM}} \quad (6)$$

where,  $i$  = Flux of gas, mol/m<sup>2</sup>.s;  $A_m$  = Area, m<sup>2</sup>;  $t$  = time, s and  $i$  = referred to as CO<sub>2</sub> Permeability of the membrane,  $P_i$ .<sup>31</sup>

$$P_i = \frac{N_i}{\Delta P_i} \quad (7)$$

where,  $P_i$  = Permeability of membrane, mol/m<sup>2</sup>. s. Pa and  $\Delta P_i$  = Pressure difference across the membrane, Pa.

## 2.7 Attenuated Total Reflectance Fourier Transform Infrared Spectroscopy

The attenuated total reflectance fourier transform infrared spectroscopy (ATR-FTIR) (NICOLET IS10, USA) was utilised to ascertain and comprehend the membrane's structure. No sample preparation was needed. Thus, a Thermo Scientific Fourier was used to test the samples and convert the infrared spectrometer within the range of 425 cm<sup>-1</sup>–4,000 cm<sup>-1</sup>. Using a diamond crystal, spectra were obtained from 32 scans at a resolution of 4 cm<sup>-1</sup> and an incident angle of 45°.

## 2.8 Sorption Study

The sorption study was conducted based on Jawad et al. in which a PerkinElmer Thermogravimetric analysis (TGA) (EXSTAR-6300, USA) was used.<sup>32</sup> Approximately 1.0 mg of MMM was placed in the TGA pan and heated with nitrogen gas at a flow rate of 30 mL/min to remove any moisture or CO<sub>2</sub>. Subsequently a heating rate of 10°C/min was applied to the samples for 5 min in order to reach 130°C. The sample was then cooled to 27°C and exposed to CO<sub>2</sub> gas at a constant flow rate of 30 mL/min. The TGA continuously measured changes in the sample's weight every 9 s at a concentration of  $C_t$ , indicating the amount of CO<sub>2</sub> being adsorbed. The concentration reached  $C_\infty$  after 65 min. This data was recorded using Pyris software linked to the PerkinElmer TGA system. The material successfully adsorbed CO<sub>2</sub> but the nitrogen gas was not adsorbed because of its low solubility in the material. The error analysis method introduced

by Barner was applied to examine membrane diffusion.<sup>33</sup> In this model,  $M_t$  represents the total amount of diffused substance entering the film at time  $t$  and  $M_\infty$  denotes the corresponding amount at  $t = \infty$ .  $M_t/M_\infty$  can also be expressed as shown in Equation (9):<sup>34</sup>

$$\frac{M_t}{M_\infty} = 1 - \frac{8}{\pi^2} \sum_{n=0}^{n=\infty} \frac{1}{(2n+1)^2} \exp\left[-\frac{D(2n+1)^2 \pi^2 t}{l^2}\right] \quad (9)$$

In this current study, Matrix laboratory (MATLAB) was utilised to solve Equation (9) to determine the CO<sub>2</sub> Diffusivity coefficient (D). Meanwhile, the value of CO<sub>2</sub> Solubility coefficient ( $S$ ) was calculated by using Equation (10) where  $S$  is expressed in cm<sup>3</sup> (STP)/cm<sup>4</sup> (cm Hg) and the gas permeation ( $P$ ) denoted in gas permeance unit (GPU).

$$P = D \times S \quad (10)$$

### 3. RESULTS AND DISCUSSIONS

#### 3.1 Hansen Solubility Parameters

The HSP analysis was conducted to assess the compatibility of materials for specific components. In this work, the HSP study was utilised mainly to perform the compatibility between the CAB polymers with the chloroform solvent and MWCNTs-F. The compatibility of materials was analysed based on the cohesive energy within the respective materials. The absolute and normalised HSP values for the polymer, solvent and inorganic filler are tabulated in Table 2. The normalised values were calculated using the above HSP Equation (1) to Equation (3) and plotted on the HSP ternary graph, as depicted in Figure 1. This graph was used to illustrate the compatibility of the materials qualitatively. As shown in Figure 1, the positions of both the CAB and chloroform are significantly closer to each other compared to MWCNTs-F. This can be validated by observing the quantitative values in Table 2 where the CAB and chloroform values are much closer. The closer the points in the ternary graph, the greater the compatibility of the materials, leading to an increase in gas permeation. Additionally, the MWCNTs-F exhibit significant properties, including high mechanical strength as well as the ability to mediate and enhance CO<sub>2</sub> diffusion behaviour in the membrane.

Table 2: Absolute and normalise HSP values for each component.

| Components | Absolute HSP values |            |            | Normalise HSP values |            |            | References | Colour |
|------------|---------------------|------------|------------|----------------------|------------|------------|------------|--------|
|            | $\delta d$          | $\delta p$ | $\delta h$ | $\delta d$           | $\delta p$ | $\delta h$ |            |        |
| CAB        | 22.09               | 6.73       | 5.22       | 64.89                | 19.8       | 15.3       | 35         | Black  |
| Chloroform | 17.80               | 3.10       | 5.70       | 66.92                | 11.7       | 21.4       | 36         | Green  |
| MWCNTs-F   | 25.64               | 5.83       | 18.00      | 51.80                | 11.8       | 36.4       | 37         | Red    |

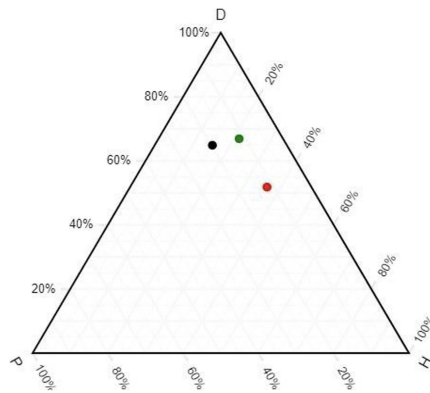


Figure 1: Ternary Plot – CAB (black dot), chloroform (green dot) and MWCNTs (red dot).

In this study, it was also observed that when the concentration of inorganic fillers was increased within the MMM structure from 0.1 wt.%–0.5 wt.%, the distance between the MWCNTs-F and the two materials in the HSP ternary graph decreased. As a result, the relative affinity decreases from 11.20 to 11.15 as displayed in Table 3. This was due to the increased the loadings of MWCNTs in the MMM, which provided more surface area for potential bonding or entanglement with the CAB polymer chains. This led to an improved dispersion and a more homogenous composite. Thus, the MWCNT was closer and compatible to CAB and the chloroform particles in the ternary plot. However, beyond a certain concentration, increasing MWCNTs could decrease the affinity. This was due to aggregation of MWCNTs caused by the strong Van der Waals forces. At higher concentrations, this aggregation became more severe impacted their interaction with CAB and resulted in poor dispersion.<sup>38</sup> Furthermore, increasing MWCNTs-F within the CAB polymer can lead to changes in the membrane thickness.<sup>39</sup> Hence, an average thickness of each membrane was recorded, as shown in Figure 2. This was because the membrane thickness directly affected the gas separation performance. As observed in Figure 2, the average thickness of M-0.1, M-0.2, M-0.3 and M-0.4 are 91.8  $\mu\text{m}$ , 155  $\mu\text{m}$ ,

179.5  $\mu\text{m}$  and 197  $\mu\text{m}$ , respectively. In contrast, M-0.5 exhibited a notably thinner profile than M-0.2 to M-0.4, with an average thickness of 144  $\mu\text{m}$ . This could possibly be due to the agglomeration caused by the increase in the MWCNTs-F content and also by the Van der Waals forces weakening the membrane.<sup>39</sup>

Table 3: Relative Affinity for respective membranes.

| Membrane name | CAB (Mn)   |            |            | Chloroform (ml) | MWCNTs-F(g) | Relative Affinity |
|---------------|------------|------------|------------|-----------------|-------------|-------------------|
|               | 12,000 (g) | 16,000 (g) | 70,000 (g) |                 |             |                   |
| M-0.1         | 0.8        | 1.6        | 1.6        | 64.34           | 0.128       | 11.20             |
| M-0.2         | 0.8        | 1.6        | 1.6        | 64.25           | 0.264       | 11.22             |
| M-0.3         | 0.8        | 1.6        | 1.6        | 64.15           | 0.412       | 11.20             |
| M-0.4         | 0.8        | 1.6        | 1.6        | 64.05           | 0.566       | 11.18             |
| M-0.5         | 0.8        | 1.6        | 1.6        | 63.94           | 0.734       | 11.15             |

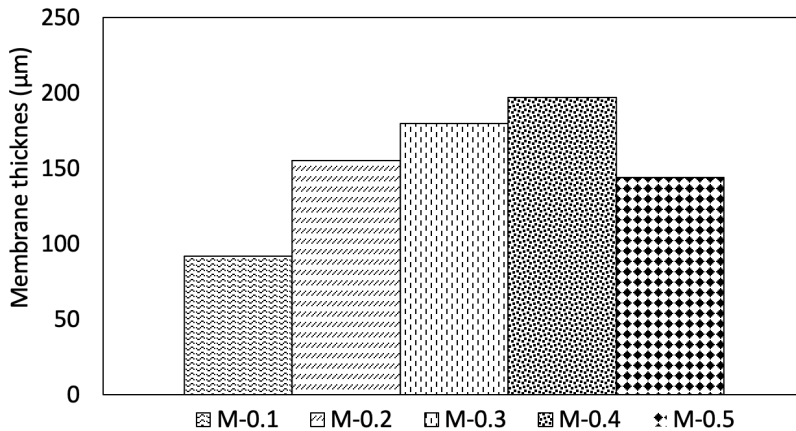


Figure 2: The thickness of the membrane at respective MWCNTs-F loading.

### 3.2 Characteristics of MMM at different loadings of MWCNTs-F

Two types of analyses were performed to evaluate the characteristics of the membranes. Firstly, an ATR-FTIR analysis was conducted to investigate the functional groups based on the different loadings of MWCNTs-F. Figure 3 displays the ATR-FTIR spectrum data. The transmittance value for C-H stretching was highest at 2,955  $\text{cm}^{-1}$ .<sup>40</sup> The transmittance band for the carbonyl group of carboxylic acid (C=O) was at 1,750  $\text{cm}^{-1}$ , while the band for the hydroxyl group (O-H) was observed at 1,360  $\text{cm}^{-1}$ . Meanwhile, the transmittance at 1,235  $\text{cm}^{-1}$  and 1,032  $\text{cm}^{-1}$  represented the stretching of acrylate (C-O) and

the C-O-C groups, respectively.<sup>41</sup> In the ATR-FTIR analysis, an aromatic carbon ring (=C-H) functional group was identified due to the presence of MWCNTs-F, with the transmittance band observed at  $2,875\text{ cm}^{-1}$ .<sup>42</sup>

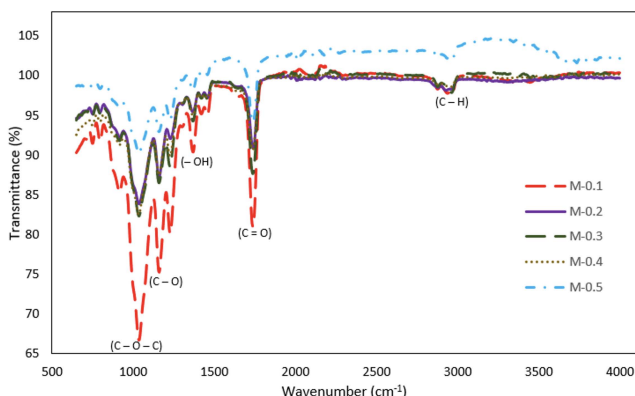


Figure 3: FTIR Results of membranes M-0.1, M-0.2, M-0.3, M-0.4 and M-0.5.

Figure 3 shows that M-0.1 exhibit the lowest frequency vibration bands through the FTIR analysis. These frequencies indicate the low presence of C=O and O-H bonds within the membrane. Due to this, the respective membrane is expected to have a lower selectivity of  $\text{CO}_2$  molecules because of the lower C=O and O-H functional groups. As a result, the interaction between the high polar molecules and the non-polar molecules was significantly low. On the other hand, the high presence of functional groups such as C=O and O-H favoured the  $\text{CO}_2$  absorption through interactions between the polar and non-polar groups which is expected to increase the  $\text{CO}_2$  permeance within the MMM.<sup>43</sup>

### 3.3 Gas Separation Performance of MMM towards $\text{CO}_2$ Gas

The performance of each MMM was first evaluated by using  $\text{CO}_2$  permeance. Figure 4 demonstrates the results of the membranes, highlighting the highest and lowest  $\text{CO}_2$  permeance values. It was observed that the  $\text{CO}_2$  permeance gradually decreased as the MWCNTs-F loading increased from 0.1 wt.% (M-0.1), 0.2 wt.% (M-0.2), 0.3 wt.% (M-0.3), 0.4 wt.% (M-0.4) to 0.5 wt.% (M-0.5). This was validated by observing that the  $\text{CO}_2$  permeances were 5,958.27 GPU (M-0.1), 2,552.84 GPU (M-0.2), 868.07 GPU (M-0.3) and 121.11 GPU (M-0.4). All these results were obtained at an average pressure of 1 bar to 3 bar and at ambient temperature. The effect of inlet pressure on the performance of the membrane was insignificant which confirmed the un-plasticisation between the blend MMM (CAB/MWCNTs) and the gas.<sup>30</sup>

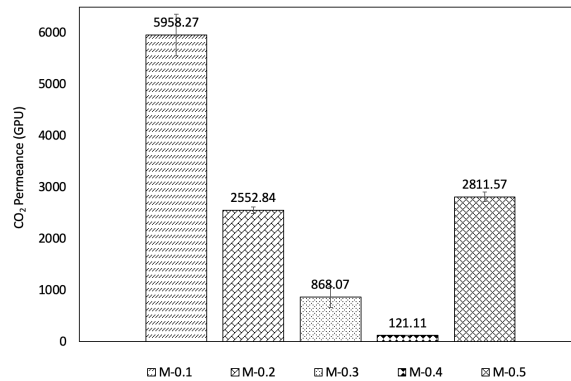


Figure 4: CO<sub>2</sub> permeance at different loadings of MWCNTs-F and at an average pressure of 1 to 3 bars.

The decrease in CO<sub>2</sub> permeance was due to the increase in the thickness of the membrane. As the loading of MWCNTs-F increased, the membrane's thickness increased as well. This can be observed in Figure 2. Thus, high loadings of inorganic filler into the membrane resulted in lower permeance.<sup>18, 32</sup> On the other hand, the CO<sub>2</sub> permeance of M-0.5 illustrated a significant increase at a value of 2,811.57 GPU. This could be attributed to the poor particle distribution and interfacial compatibility of the MWCNTs-F incorporated in the blend CAB MMM.<sup>44</sup> These findings were consistent with those of Ahmed et al. who demonstrated that optimal CO<sub>2</sub> permeance can be achieved by incorporating the best loading of functionalised MWCNTs within the membrane structure.<sup>27</sup>

Importantly, the CO<sub>2</sub> solubility and diffusivity coefficients for the MMMs were calculated and presented in Table 4. It was observed that when the CO<sub>2</sub> permeance decreased from 5,958.27 GPU (M-0.1) to 2,552.84 GPU (M-0.2) and to 121.11 GPU (M-0.4), and then increased to 2,811.57 GPU (M-0.5), the CO<sub>2</sub> solubility coefficient in cm<sup>3</sup>(STP)/cm<sup>4</sup>.cmHg reduced from  $2.19 \times 10^8$  to  $3.64 \times 10^7$  and  $1.24 \times 10^6$  then increased to  $1.44 \times 10^8$ . This behaviour in chain spacing was directly related to the solution diffusion ability as it influenced mass transfer efficiency, which in turn affected the CO<sub>2</sub> sorption.<sup>18</sup>

The sudden reduction in the CO<sub>2</sub> permeance from 2,552.84 GPU (M-0.2) to 121.11 GPU (M-0.3) caused a significant reduction of the CO<sub>2</sub> diffusivity coefficient from  $7.02 \times 10^{-5}$  cm<sup>2</sup>/s to  $4.55 \times 10^{-7}$  cm<sup>2</sup>/s. This decrease in the CO<sub>2</sub> diffusivity coefficient was mainly due to the lowering of the amorphous fraction and shortening of the chain spacing.<sup>18</sup> Thus, when the CO<sub>2</sub> diffusivity increased, the chain spacing reduced, which hindered the gas diffusion within

the membrane structure. Hence, it has been proven that the driving force for this newly synthesised MMM from CAB with Mn of 12,000, 16,000 and 70,000 is mostly the CO<sub>2</sub> solubility coefficient.

Table 4: CO<sub>2</sub> solubility and diffusivity coefficients of MMM.

| Membrane | CO <sub>2</sub> Diffusivity coefficient (cm <sup>2</sup> /s) | CO <sub>2</sub> Solubility coefficient (cm <sup>3</sup> (STP)/cm <sup>4</sup> .cmHg) |
|----------|--|--|
| M-0.1    | $2.73 \times 10^{-5}$  | $2.19 \times 10^8$   |
| M-0.2    | $7.02 \times 10^{-5}$  | $3.64 \times 10^7$   |
| M-0.3    | $4.55 \times 10^{-7}$  | $1.91 \times 10^6$   |
| M-0.4    | $9.76 \times 10^{-5}$  | $1.24 \times 10^6$   |
| M-0.5    | $1.95 \times 10^{-5}$  | $1.44 \times 10^8$   |

Furthermore, the CO<sub>2</sub> solubility and diffusivity coefficients of MMM-0.1 was compared with the findings from previous studies, as tabulated in Table 5. It was found that the CO<sub>2</sub> diffusivity and solubility coefficients of MMM-0.1 were lower than the literature.<sup>13, 18, 32</sup> This discrepancy might be attributed to the best loading of MWCNTs (0.1 wt.%) used in this work, which was lower than 0.8 wt.% as reported in previous studies. This difference could be due to the compatibility of the CAB matrix, which resulted from the variations in the molecular weight of blend CAB polymers or the acetyl content of the cellulose acetate (CA) polymer. In fact, lower MWCNT loading could potentially lead to reduce CO<sub>2</sub> transport pathways and decrease solubility.<sup>45</sup>

Table 5: A comparison table summarising CO<sub>2</sub> solubility and diffusivity coefficients of MMMs.

| Polymer (Mn) | Polymer (wt.%) [Ratio]                  | Filler of MWCNTs-F (wt.%) | CO <sub>2</sub> Diffusivity coefficient (cm <sup>2</sup> /s) | CO <sub>2</sub> Solubility coefficient (cm <sup>3</sup> (STP)/cm <sup>4</sup> .cmHg) | Reference     |
|--------------|---|---------------------------|--|--|---------------|
| CAB          | 4<br>(2:1:1 of Mn<br>12000:16000:70000) | 0.1                       | $2.73 \times 10^{-5}$  | $2.19 \times 10^8$   | Present study |
| CAB          | 4<br>(2:1 of Mn 70000:12000)            | 0.8                       | $4.0 \times 10^{-11}$  | $9.24 \times 10^{12}$  | 18            |
| CA           | 15<br>(CA of 39% acetyl)                | 0.1                       | $6.8 \times 10^{-12}$  | $14.96 \times 10^{13}$   | 13            |
| CA           | 10<br>(CA of 54.6–56% acetyl)           | 0.1                       | $3.7 \times 10^{-11}$  | $198.35 \times 10^{11}$  | 32            |

#### 4. CONCLUSION

This research explored integration of CAB with Mn of 12,000, 16,000 and 70,000 in the ratio of 1:2:2 along with different loadings of MWCNTs-F to investigate the CO<sub>2</sub> diffusivity and solubility coefficients in the MMMs. Based on the HSP, it was observed that the CAB and chloroform solvent exhibited higher compatibility in comparison to MWCNTs. Additionally, the study revealed a direct relationship between CO<sub>2</sub> permeance and CO<sub>2</sub> solubility coefficients. When the CO<sub>2</sub> permeance of the MMM decreases from 5,958.27 GPU to 121.11 GPU, the CO<sub>2</sub> solubility coefficient also decreased from  $2.19 \times 10^8$  to  $1.24 \times 10^6$  cm<sup>3</sup>(STP)/cm<sup>4</sup>.cmHg due to the solution diffusion mechanism. Future studies could explore the integration of CAB with different molecular weights and MWCNTs-F to further improve the sorption coefficients.

#### 5. ACKNOWLEDGEMENTS

The authors gratefully acknowledge the financial support provided by The International Research Collaboration Co-Fund (IRCC) with award number CENG-IRCC-2023-110 from Qatar University.

#### 6. REFERENCE

1. Ahmad, A. L., Olatunji, S. & Jawad, Z. (2017). Thickness effect on the morphology and permeability of CO<sub>2</sub>/N<sub>2</sub> gases in asymmetric polyetherimide membrane. *J. Phys. Sci.*, 28(Supp. 1), 201–213. <https://doi.org/10.21315/jps2017.28.s1.13>
2. Ming, W. et al. (2024). Blend cellulose acetate butyrate membrane with molecular weight 12,000, 30,000 and 65,000 for CO<sub>2</sub>/N<sub>2</sub> separation. *J. Phys. Sci.*, 35(1), 35–51. <https://doi.org/10.21315/jps2024.35.1.4>
3. Sugu, L. & Jawad, Z. A. (2019). Formation of low acetyl content cellulose acetate membrane for CO<sub>2</sub>/N<sub>2</sub> separation. *J. Phys. Sci.*, 30(1), 111–125. <https://doi.org/10.21315/jps2019.30.1.9>
4. Asif, K. et al. (2023). A molecular simulation study on amine-functionalized silica/polysulfone mixed matrix membrane for mixed gas separation. *Chemosphere*, 311, 136936. <https://doi.org/10.1016/j.chemosphere.2022.136936>
5. Baker, R. W. (2002). Future Directions of Membrane Gas Separation Technology. *Ind. Eng. Chem. Res.*, 41(6), 1393–1411. <https://doi.org/10.1021/ie0108088>
6. Taheri Najafabadi, A. (2013). CO<sub>2</sub> chemical conversion to useful products: An engineering insight to the latest advances toward sustainability. *Int. J. Energy Res.*, 37(6), 485–499. <https://doi.org/10.1002/er.3021>
7. Jin, R. P. W. X. et al. (2020). Preparation and characterisation of blend cellulose acetate membrane for CO<sub>2</sub>/N<sub>2</sub> separation. *J. Phys. Sci.*, 31(2), 15–31. <https://doi.org/10.21315/jps2020.31.2.2>

8. Ismail, A. F. & David, L. I. B. (2001). A review on the latest development of carbon membranes for gas separation. *J. Membr. Sci.*, 193(1), 1–18. [https://doi.org/10.1016/S0376-7388\(01\)00510-5](https://doi.org/10.1016/S0376-7388(01)00510-5)
9. Ng, S.C. et al. (2020). Influence of polymer blending of cellulose acetate butyrate for CO<sub>2</sub>/N<sub>2</sub> separation. *J. Phys. Sci.*, 31(1), 69–84. <https://doi.org/10.21315/jps2020.31.1.5>
10. Chong, D. et al. (2020). The influence of blending different molecular weights of cellulose acetate butyrate for CO<sub>2</sub>/N<sub>2</sub> separation. *J. Phys. Sci.*, 31(2), 91–112. <https://doi.org/10.21315/jps2020.31.2.7>
11. Lee, R. J. et al. (2018). Incorporation of functionalized multi-walled carbon nanotubes (MWCNTs) into cellulose acetate butyrate (CAB) polymeric matrix to improve the CO<sub>2</sub>/N<sub>2</sub> separation. *Process Saf. Environ. Prot.*, 117, 159–167. <https://doi.org/10.1016/j.psep.2018.04.021>
12. Ngo, J. Q. et al. (2020). The influence of cellulose acetate butyrate membrane structure on the improvement of CO<sub>2</sub>/N<sub>2</sub> separation. *Chem. Eng. Commun.*, 207(12), 1707–1718. <https://doi.org/10.1080/00986445.2019.1680365>
13. Wong, E. T. S. et al. (2018). A kinetic study of CO<sub>2</sub> sorption improvement in the CA-CNTs mixed matrix membrane. *IOP Conf. Ser.: Mater. Sci. Eng.*, 458, 012066. <https://doi.org/10.1088/1757-899X/458/1/012066>
14. Bahreini, H., Ameri, E. & Ebadi-Dehaghani, H. (2024). Effect of incorporation of multi-walled carbon nanotubes on the CO<sub>2</sub>/CH<sub>4</sub> separation performance of sulfonated poly (ether ether ketone) / polyetherimide composite membranes using design of experiments and molecular dynamics simulation methods. *Arabian J. Chem.*, 17(1), 105400. <https://doi.org/10.1016/j.arabjc.2023.105400>
15. Chen, J. et al. (2014). Effect of molecular structure on the gas permeability of cellulose aliphate esters. *Chin. J. Polym. Sci.*, 32(1), 1–8. <https://doi.org/10.1007/s10118-014-1384-2>
16. Juber, F. A. H. et al. (2021). The prospect of synthesis of PES/PEG blend membranes using blend NMP/DMF for CO<sub>2</sub>/N<sub>2</sub> separation. *J. Polym. Res.*, 28(5), 177. <https://doi.org/10.1007/s10965-021-02500-6>
17. Manimaran, D., Jawad, Z. & Chew, T. L. (2019). Effect of solvent evaporation time and casting thickness on the separation performance of cellulose acetate butyrate blend membrane. *J. Appl. Membr. Sci. Technol.*, 23(2). <https://doi.org/10.11113/amst.v23n2.151>
18. Lee, R. J. et al. (2020). Blend cellulose acetate butyrate/functionalised multi-walled carbon nanotubes mixed matrix membrane for enhanced CO<sub>2</sub>/N<sub>2</sub> separation with kinetic sorption study. *J. Environ. Chem. Eng.*, 8(5), 104212. <https://doi.org/10.1016/j.jece.2020.104212>
19. Anbealagan, L. D. et al. (2021). Modified zeolite/polysulfone mixed matrix membrane for enhanced CO<sub>2</sub>/CH<sub>4</sub> separation. *Membranes*, 11(8), 630. <https://doi.org/10.3390/membranes11080630>
20. Goh, P. S. et al. (2011). Recent advances of inorganic fillers in mixed matrix membrane for gas separation. *Sep. Purif. Technol.*, 81(3), 243–264. <https://doi.org/10.1016/j.seppur.2011.07.042>

21. Zhang, Y. et al. (2013). Current status and development of membranes for CO<sub>2</sub>/CH<sub>4</sub> separation: A review. *Int. J. Greenhouse Gas Con.*, 12, 84–107. <https://doi.org/10.1016/j.ijggc.2012.10.009>
22. Andecochea Saiz, C. et al. (2018). Shortcut applications of the Hansen Solubility Parameter for Organic Solvent Nanofiltration. *J. Membr. Sci.*, 546, 120–127. <https://doi.org/10.1016/j.memsci.2017.10.016>
23. Lapuerta, M. & Canoira, L. (2016). Chapter 4 - The Suitability of Fatty Acid Methyl Esters (FAME) as Blending Agents in Jet A-1. In C. J. Chuck (Ed.). *Biofuels for Aviation*. Academic Press, 47–84. <https://doi.org/10.1016/B978-0-12-804568-8.00004-4>
24. Ahmad, A. L. et al. (2013). The functionalization of beta-cyclodextrins on multi walled carbon nanotubes: Effects of the dispersant and non aqueous media. *Curr. Nanosci.*, 9(1), 93–102. <https://doi.org/10.2174/157341313805117839>
25. Shuba, M. V. et al. (2012). Soft cutting of single-wall carbon nanotubes by low temperature ultrasonication in a mixture of sulfuric and nitric acids. *Nanotechnol.*, 23(49), 495714. <https://doi.org/10.1088/0957-4484/23/49/495714>
26. Jawad, Z. et al. (2017). Binding stability of β-CD on MWCNTS: Role of washing cycle on the β-CD coating. *J. Phys. Sci.*, 28(Supp. 1), 145–153. <https://doi.org/10.21315/jps2017.28.s1.9>
27. Ahmad, A. L. et al. (2014). A cellulose acetate/multi-walled carbon nanotube mixed matrix membrane for CO<sub>2</sub>/N<sub>2</sub> separation. *J. Membr. Sci.*, 451, 55–66. <https://doi.org/10.1016/j.memsci.2013.09.043>
28. Mokhtari, F. et al. (2021). Recent advances of polymer-based piezoelectric composites for biomedical applications. *J. Mech. Behav.*, 122, 104669. <https://doi.org/10.1016/j.jmbbm.2021.104669>
29. Hansen, C. M. (2007). *Hansen Solubility Parameters* (2nd ed.). CRC Press, 544. <https://doi.org/10.1201/9781420006834>
30. Lee, S., Pang, J. & Jawad, Z. (2019). Functionalised multi-walled carbon nanotubes/cellulose acetate butyrate mixed matrix membrane for CO<sub>2</sub>/N<sub>2</sub> separation. *J. Phys. Sci.*, 30(2), 99–135. <https://doi.org/10.21315/jps2019.30.2.7>
31. Sadrzadeh, M., Rezakazemi, M. & Mohammadi, T. (2018). Fundamentals and Measurement Techniques for Gas Transport in Polymers. In S. Thomas et al. (Ed.). *Transport Properties of Polymeric Membranes*. Elsevier, 391–423. <https://doi.org/10.1016/B978-0-12-809884-4.00019-7>
32. Jawad, Z. A. et al. (2015). Influence of solvent exchange time on mixed matrix membrane separation performance for CO<sub>2</sub>/N<sub>2</sub> and a kinetic sorption study. *J. Membr. Sci.*, 476, 590–601. <https://doi.org/10.1016/j.memsci.2014.11.008>
33. Barnes, C. (1934). Diffusion Through a Membrane. *Phys.*, 5, 4–8. <https://doi.org/10.1063/1.1745209>
34. Crank, J. (1975). *The Mathematics of Diffusion*. Oxford: Clarendon Press. 399–406.
35. Ramanaiah, S., Reddi Rani, P. & Reddy, K. (2012). Hansen solubility parameters for the solid surface of cellulose acetate propionate by inverse gas chromatography. *J. Macromol. Sci. Part B Phys.*, 51(11), 2191–2200. <https://doi.org/10.1080/00222348.2012.669681>

36. Hansen, A. (2018). *Environment, Media and Communication*. London: Routledge. <https://doi.org/10.4324/9781315625317>
37. Ma, J. et al. (2018). Dispersion of pristine and polyaniline functionalized carbon nanotubes in designed solvent mixtures by Hansen solubility parameters. *Mater. Today Commun.*, 14, 99–105. <https://doi.org/10.1016/j.mtcomm.2017.12.017>
38. Dubey, R. et al. (2021). Functionalized carbon nanotubes: Synthesis, properties and applications in water purification, drug delivery, and material and biomedical sciences. *Nanoscale Adv.*, 3(20), 5722–5744. <https://doi.org/10.1039/D1NA00293G>
39. Abdelsalam, A. et al. (2020). The influence of embedding different loadings of MWCNTs on the structure and permeation of CAB blended membrane. *J. Phys. Sci.*, 31(1), 15–36. <https://doi.org/10.21315/jps2020.31.1.2>
40. Lavorgna, M. et al. (2013). Silanization and silica enrichment of multiwalled carbon nanotubes: Synergistic effects on the thermal-mechanical properties of epoxy nanocomposites. *Eur. Polym. J.*, 49(2), 428–438. <https://doi.org/10.1016/j.eurpolymj.2012.10.003>
41. Del Valle, E. M. M. (2004). Cyclodextrins and their uses: A review. *Process Biochem.*, 39(9), 1033–1046. [https://doi.org/10.1016/S0032-9592\(03\)00258-9](https://doi.org/10.1016/S0032-9592(03)00258-9)
42. Suttiwijitpukdee, N. et al. (2011). Intermolecular interactions and crystallization behaviors of biodegradable polymer blends between poly (3-hydroxybutyrate) and cellulose acetate butyrate studied by DSC, FT-IR, and WAXD. *Polymer*, 52(2), 461–471. <https://doi.org/10.1016/j.polymer.2010.11.021>
43. Bae, Y.-S. & Snurr, R. Q. (2011). Development and evaluation of porous materials for carbon dioxide separation and capture. *Angew. Chem. Int. Ed.*, 50(49), 11586–11596. <https://doi.org/10.1002/anie.201101891>
44. Mahajan, R. & Koros, W. J. (2000). Factors controlling successful formation of mixed-matrix gas separation materials. *Ind. Eng. Chem. Res.*, 39(8), 2692–2696. <https://doi.org/10.1021/ie990799r>
45. Zhang, H. et al. (2016). Mixed-matrix membranes containing carbon nanotubes composite with hydrogel for efficient CO<sub>2</sub> separation. *ACS Appl.*, 8(42), 29044–29051. <https://doi.org/10.1021/acsami.6b09786>